Journal of Magnetic Resonance **149,** 103–109 (2001)
doi:10.1006/jmre.2000.2275, available online at http://www.idealibrary.com on IDEAL®

Symmetric Echo Acquisition for Absolute-Value Display in Solid-State NMR Imaging

S. Matsui[1] and S. Saito

Institute of Applied Physics, University of Tsukuba, Tsukuba, Ibaraki 305-8573, Japan

Received October 11, 2000; revised December 4, 2000

A method of solid-state NMR imaging that permits echo Fourier transformation (FT) has been devised using a magic echo train. The echo FT imaging can be implemented simply by modifying the gradient pulse sequence in the previous magic echo imaging (TREV-16TS) so that the one-dimensional *k*-space trajectory follows the sampling points which are symmetric about the *k* origin. The implemented ability of echo FT improves the performance of the magic echo imaging: the sensitivity gained by $\sqrt{2}$, the phase correction is made unnecessary, and the digital resolution is doubled. One- and two-dimensional imaging experiments have been conducted on some solid samples, confirming the improved performance and revealing a TREV-16TS adjustment parameter that is critical for the successful echo FT imaging.

Key Words: **solid-state imaging; echo Fourier transformation; *k*-space; absolute value display; magic echo.**

INTRODUCTION

In liquid-state MRI, imaging signals are generally acquired in the form of an echo rather than an FID. This is due to the well-known fact that Fourier transformation (FT) of the echo signal, which is an even function in the time domain, leads to a null imaginary component (dispersion) in the frequency domain, permitting the use of the absolute value for real component (absorption) display without worrying about the phase correction (*1*). This is in contrast to the case of FID acquisition where the nonzero imaginary component renders the phase correction indispensable and results in degrading the spatial resolution if the absolute-value display is employed. Thus, the signal acquisition in the echo form is beneficial to obtain high-quality images that are completely free from phase errors, tacitly contributing to the success in the biomedical application of liquid-state MRI.

On the other hand, in solid-state MRI, which appears promising in the application to material characterization, an FID is usually acquired and few experiments are reported on the echo acquisition. This can probably be ascribed to the fact that attention has been paid exclusively to the main problem in solid-state MRI, i.e., effective quenching of the strong dipolar interaction. In addition, the echo acquisition while effectively quenching the dipolar interaction is technically much more demanding than the simple echo acquisition in liquid-state MRI. To our knowledge, the only echo experiment on a solid sample published so far is the Hahn spin-echo imaging experiment using a 180° pulse under the MREV-8 line narrowing (*2*). With the echo signal obtained by this type of echo acquisition, however, it is easier to lose the symmetry unless a high degree of line narrowing is achieved, resulting in an incomplete zeroing of the imaginary component.

In this paper, we propose a method of solid-state MRI that enables the echo acquisition under the magic-echo line narrowing (*3–14*). Due to the sophisticated way of acquisition, the method allows a highly symmetric echo to be acquired under relatively poor line-narrowing conditions, in contrast to the simple echo acquisition mentioned above. Our discussion here is restricted to the magic-echo line narrowing approach, although similarly sophisticated ways of acquisition may be conceivable with some other types of line-narrowing techniques. After illustrated by using the trajectory in the so-called *k*-space, the sophisticated echo acquisition will be tested by 1D and 2D magic-echo imaging experiments performed on natural rubber, plastic solid, and polymer samples. The method proposed here will improve the performance of the solid-state imaging, activating further the application of MRI to material characterization.

SYMMETRIC ECHO ACQUISITION IN MAGIC ECHO IMAGING

Figure 1a shows the magic-echo pulse sequence for solid-state imaging (TREV-16TS) (*3–14*). Details of the line-narrowing mechanism were described by Rhim *et al.* (*15*) and by Takegoshi and McDowell (*16*). To improve the line-narrowing efficiency, a 180° y (or 180° $-y$) pulse is virtually inserted into each RF burst by using identical 90° y (or 90° $-y$) pulses for the sandwiching (*3, 5*). The virtual 180° pulse refocuses relatively weak inhomogeneous interactions like chemical shift and additionally some experimental imperfections of the pulse sequence that are proportional to spin operator I_Z, leading to a highly efficient line narrowing. In the previously proposed method, the polarity of the gradient G, applied during every RF-free window, was inverted periodically as indicated by (A) in Fig. 1a to preserve

[1] To whom correspondence should be addressed. E-mail: matsui@bk.tsukuba.ac.jp.

1090-7807/01 $35.00

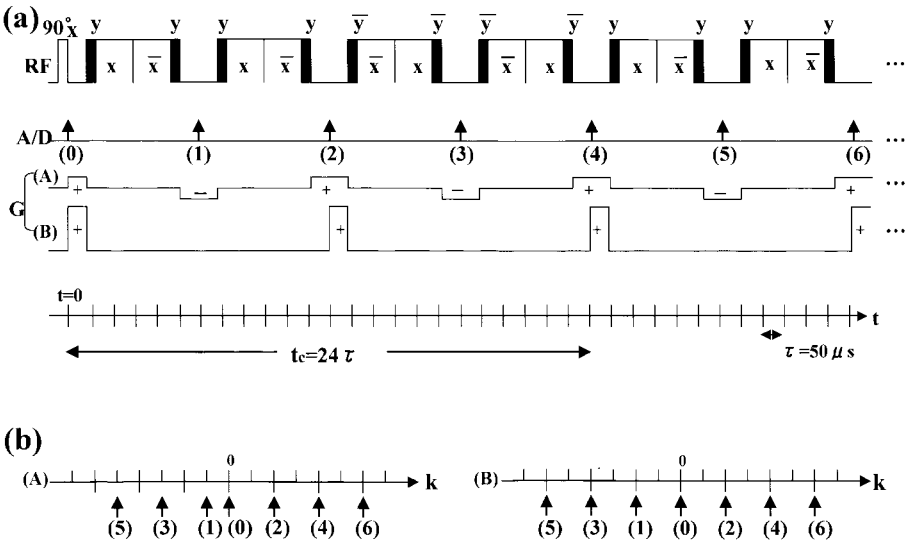

FIG. 1. Pulse sequences for magic echo solid-state NMR 1D imaging (TREV-16TS) (a), and the corresponding signal sampling points in the 1D *k*-space (b). Note that while the 1D *k* trajectory (A) obtained with the gradient sequence G(A) is not symmetric about the *k* origin, the 1D *k* trajectory (B) followed by using the modified gradient sequence G(B) is symmetric. This modification, in which the gradient amplitude is increased four times to obtain the same FOV, allows a symmetric echo signal to be acquired. See text for further details.

the gradient effect under the action of the virtually applied 180° pulses (*3, 5, 8*).

Note here that the TREV-16TS pulse sequence can be regarded as a combination of the TREV homonuclear-dipolar-decoupling line-narrowing sequence with the Meiboom–Gill (MG) sequence consisting of the virtual 180° pulses (*3, 5, 8*). This provides a hint of considering the symmetric echo acquisition analogously with that performed in liquid-state MRI using the CPMG spin-echo sequence (*17*). Namely, one notes, when the gradient pulses are absent, that the TREV homonuclear-dipolar-decoupling sequence ideally does nothing but prolong the short FID signal by quenching the homogeneous interaction and scaling the inhomogeneous interactions, as far as the signal samplings are made at magic-echo peaks in the middle of the RF-free windows (Fig. 1a). For isotropic chemical shifts, the scaling may give rise to line shifting rather than line narrowing (FID prolonging); however, they are anyway removed by the application of the MG sequence as mentioned above. The result is the conversion of the solid sample with the short FID signal to a virtually liquid sample with a much longer, single-component FID signal. Thus, the TREV-16TS sequence applied to the solid sample can be reduced to the MG sequence applied to the virtual liquid sample with the 180° pulse applied for each sandwiched RF burst.

Now, it is easy to understand that when the gradient pulses are present, the 1D *k*-space trajectories traced under the application of the TREV-16TS imaging sequences (Fig. 1a) are represented by the successive signal sampling positions in Fig. 1b. The sampling positions can be followed by considering the signal evolution in the 1D *k*-space due only to the gradient pulses and by noting that the effect of each virtual 180° pulse on the trajectories is a reflection about the *k* origin (*17*). The *k*-space trajectories indicated as (A) and (B) can thus be obtained by applying the gradient sequences (A) and (B), respectively.

Apparently, the sampling-position trajectory (A) is not symmetric with respect to the *k* origin; therefore, the even- and odd-numbered sampling points must be separately processed. They represent two distinct FIDs. Fourier transformation of these FIDs produces the images that are mutually related by a reflection about the center of the image matrix. In the previous method, the even-numbered sampling points were taken while the odd-numbered sampling points were discarded (*3, 5, 8*).

One way of complementarily using all the sampling points available within a single measurement is to employ the gradient sequence (B), having the corresponding *k*-space trajectory as shown by (B). To obtain the symmetric sampling points (B), gradient pulses are applied during the second halves of the selected RF-free windows with the pulse width set to τ. For obtaining the same field of view (FOV) as (A), the gradient amplitude is increased by a factor of 4. This gradient increase is the only shortcoming in the proposed acquisition of symmetric echo. However, since the RF-free windows can be expanded as wide as the transverse relaxation time in the magic echo imaging (*3–16*), the gradient increase does not seem so severe for the current high-speed gradient drivers if the inductance of the gradient coil is small (a few μHz).

The proposed method of echo acquisition has three advantages over the previous method of FID acquisition: (i) The sensitivity is gained by $\sqrt{2}$, since the acquired echo can be regarded as a back-to-back sum of two complementary FIDs. (ii) The digital resolution is doubled. (iii) The phase correction for the real component (absorption) display becomes unnecessary. Furthermore, compared to the simple echo acquisition based on the Hahn spin

echo (*2*), the sophisticated echo acquisition using the MG sequence can be more tolerable to the degradation of the echo symmetry associated with the decrease in the line-narrowing efficiency. This is due to the difference in the signal sampling order in the *k*-space. While in the former acquisition the transverse relaxation effect leads directly to an asymmetric echo, the effect is much smaller in the latter.

It should be mentioned here that another gradient sequence is conceivable with which the same symmetric-echo-acquisition as in (B) can in principle be achieved by using a gradient amplitude smaller than that in the gradient sequence (B). The amplitude can be reduced down to one-half that in (B) by suitably adding negative gradient pulses to the gradient sequence (B) (during the RF-free windows where the positive gradient pulses are not present). Each negative pulse must be applied only during the first half of the RF-free window and the gradient must be absent completely in the second half of that RF-free window. Unfortunately, this requires a perfect gradient switching, making this gradient sequence difficult to realize. (In fact, the gradient scheme did not work well experimentally, hindered presumably by the residual gradient immediately after switching off each negative gradient pulse.) We will not be concerned with this scheme anymore in this paper.

EXPERIMENTAL

All the experiments were performed on a homebuilt NMR imager, operating at 59.85 MHz for protons. In the TREV-16TS line-narrowing sequence (Fig. 1a), the 90° pulse length was 2.4 μs and the time interval τ was set to 50 μs. Three samples, natural rubber, adamantane, and polycarbonate, were used for the initial symmetric-echo-acquisition experiments. The relaxation times T_2 for these samples, 1 ms, 50 μs, and 30 μs, respectively, were prolonged by the line-narrowing sequence specified above to about 20, 15, and 1.5 ms. (The narrowing result for the adamantane sample is nearly twice as good as the result previously reported (*8*). This may be mainly ascribed to the better RF homogeneity due to the smaller sample volume (see Fig. 4). The worse narrowing result obtained for the polycarbonate sample, on the other hand, may be due to the fixed time interval $\tau = 50$ μs, which should be shorter for attaining a better narrowing in this sample.)

The gradient amplitude in the conventional magic echo imaging ((A) in Fig. 1) was approximately 1.6 G/cm, giving an FOV of about 9 mm. The FIDs and the echoes were sampled using respectively 60–80 and 120–160 points, depending on the sample, and zero-filled identically to 256 points before the FT. In the 2D imaging experiments, 100 projections were collected by stepwise sample rotation. Signals were accumulated four times for obtaining a projection.

RESULTS AND DISCUSSION

First, 1D and 2D imaging experiments were made on a natural rubber sample cut from a rubber tube (see Fig. 3). This sample is a liquid-like solid and useful for the preliminary test before the experiments are extended to more rigid solids. Figure 2 compares the 1D results obtained from the FID- and echo-FT experiments. The 1D images (projections), Figs. 2a, 2b, and 2c, corresponding respectively to the real component (absorption), the imaginary component (dispersion), and the absolute value display, were recorded by acquiring the FID using the conventional sequence (Fig. 1a (A)). The echo-acquisition counterparts obtained using the modified sequence (Fig. 1a (B)) are shown as Figs. 2d, 2e, and 2f.

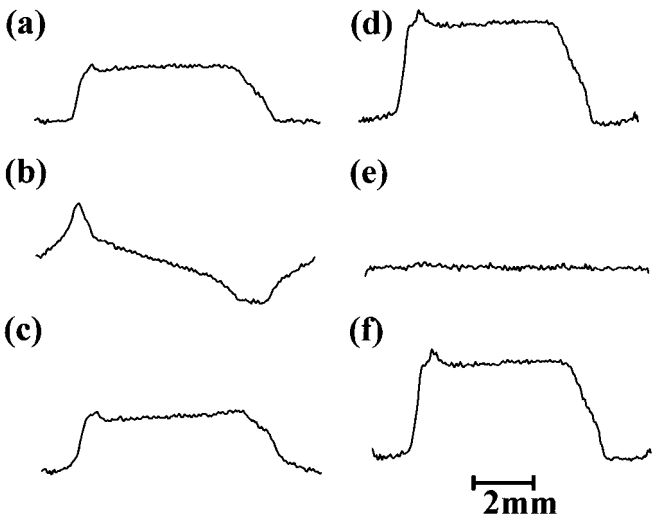

FIG. 2. Representative 1D images (projections) of the natural rubber sample (Fig. 3), plotted for comparing the echo FT with the FID FT. Projections (a), (b), and (c) correspond to the real component (absorption), the imaginary component (dispersion), and the absolute-value display obtained by using the FID acquired with the conventional gradient sequence (Fig. 1a (A)). The echo FT counterparts obtained with the modified gradient sequence (Fig. 1a (B)) are shown as projections (d), (e), and (f). Note that while the FID-FT imaginary component, (b), is nonzero, the echo-FT counterpart, (e), is completely zero. This results in the distinct absolute-value projections, (c) and (f): While the resolution is lowered in projection (c), due to the nonzero imaginary component, projection (f) is free from such a loss in resolution. It can be seen further that compared to projection (a), the signal intensity of projections (d) and (f) is doubled and the noise intensity is also increased by a factor of $\sqrt{2}$, providing a $\sqrt{2}$ gain in sensitivity.

It is clearly seen from Fig. 2 that while the FID-FT imaginary component, 2b, is nonzero, the echo-FT counterpart, 2e, is completely zero. This results in the distinct absolute-value images, 2c and 2f: While image 2c represents a projection with a lowered resolution due to the nonzero imaginary component, 2b, image 2f is free from such a loss in resolution. This allows the use of the absolute-value image, 2f, for the real component (absorption) display, eliminating the phase correction procedure necessary for the FID-FT experiment. In addition, it can be seen that the signal intensity of the projection images, 2d and 2f, is doubled compared to the projection image, 2a. This is a direct consequence of echo FT as mentioned above. Careful observation of the images in Fig. 2 will clarify another consequence of echo FT that the noise intensity is also increased by a factor of $\sqrt{2}$. The net result is a $\sqrt{2}$ gain in the sensitivity. Although not

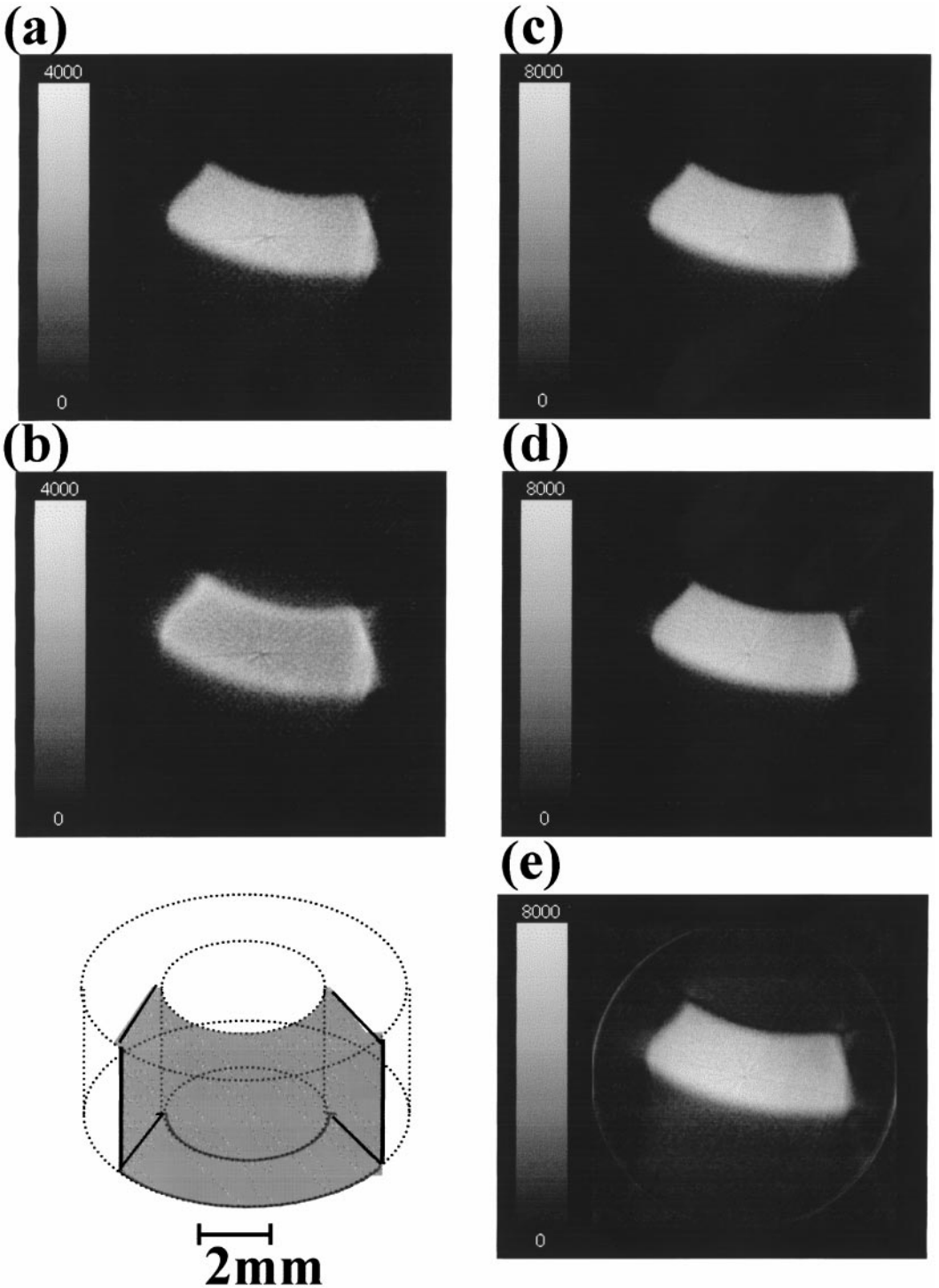

FIG. 3. Two-dimensional images of the natural rubber sample as shown by the inset, demonstrating the superiority of the echo-FT imaging to the conventional FID-FT imaging. (a) Real component and (b) absolute-value images obtained by filtered back projection (FBP) using FIDs. (c) Real component and (d) absolute-value images obtained by FBP using echoes. (e) Absolute-value image produced by 2D FT reconstruction using 2D echo data converted from the polar to the rectangular coordinate *k*-space. Note that compared to the real images (a) and (c), the absolute-value image (b) exhibits a lowered resolution while the absolute-value image (d) does not. Further, the echo-FT real and absolute-value images (c) and (d) are improved in sensitivity. The 2D FT image (e) looks equivalent to the other echo-FT images (c) and (d).

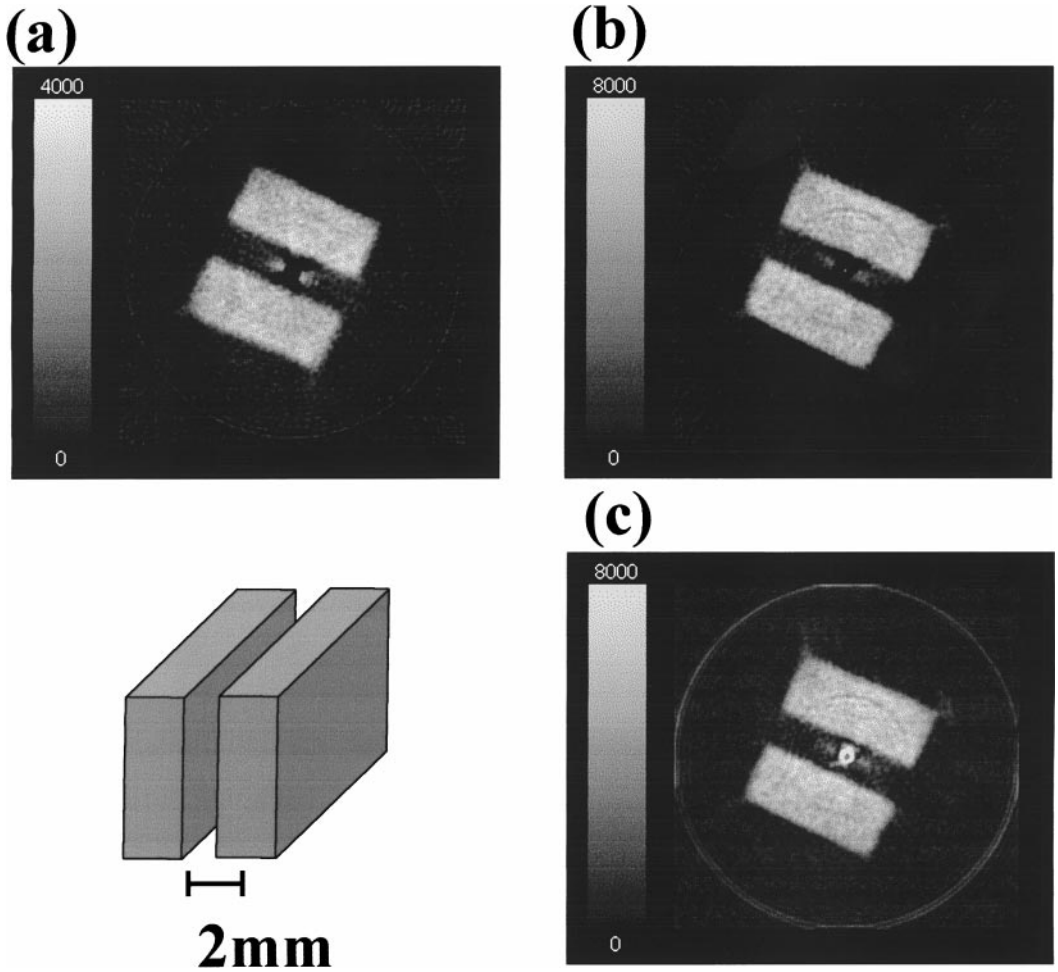

FIG. 4. Two-dimensional images of the adamantane sample as shown by the inset, demonstrating the superiority of the echo-FT imaging to the conventional FID-FT imaging. (a) FID-FT real and (b) echo-FT absolute-value images obtained by filtered back projection (FBP). (c) Absolute-value image produced by 2D FT reconstruction using 2D echo data interpolated from the polar to the rectangular coordinate *k*-space. Compared to the FID-FT image (a), the echo-FT images (b) and (c) are improved in sensitivity. Some ring and dc artifacts can be observed in all the images and their appearances are somehow different in the 2D FT image (c) due to the difference in the reconstruction algorithm. These artifacts are however not associated with the sophisticated way of echo acquisition, since they are seen in all the images.

clear from the images, the digital resolution is also doubled in the echo FT relative to the FID FT, since the number of signal sampling points is doubled in the echo acquisition.

The results of the 2D imaging experiments performed on the same rubber sample are summarized in Fig. 3, again demonstrating the superiority of the echo FT experiments. The 2D images, 3a and 3b, were obtained using FIDs, other 2D images, 3c and 3d, using echoes. These four 2D images were reconstructed from 100 projections, as exemplified in Fig. 2, by using the filtered back projection (FBP) algorithm. Compared to the phase-corrected 2D real image, 3a, the 2D absolute-value image from the FID FT, 3b, exhibits a lowered resolution. By contrast, the 2D absolute-value image from the echo FT, 3d, does not suffer from the resolution loss. Further, the echo-FT 2D real- and absolute-value images, 3c and 3d, are improved in sensitivity compared to the FID-FT 2D images, 3a and 3b.

Despite that we have employed the FBP for reconstruction of the aforementioned 2D images, it is not in the FBP but in the 2D FT reconstruction that the symmetric echo acquisition plays a more vital role: In the case of the 2D FT reconstruction, unlike in the FBP reconstruction, the absolute values are taken after completing the 2D FT. Because of the null imaginary (dispersion) components, the 2D absolute-value image thus obtained by the 2D FT reconstruction using echoes is free from the well-known phase twist problem encountered in the 2D FT processing using FIDs. Of course, there is no need to pay attention to the phase adjustment of the signal throughout the experiment as in the FBP experiment. To confirm these features of the 2D FT, we have converted the 2D data collected in the polar-coordinate *k*-space to those in the rectangular-coordinate *k*-space for 2D FT. The data conversion was made such that each rectangular point was deduced by an average of the nearest 4

polar points surrounding that rectangular point. The 2D echo-FT result is shown in Fig. 3e. A 2D absolute-value image is obtained with a resolution and sensitivity both as good as the other 2D echo-FT images, 3c and 3d, although the appearance of the ring artifact is different. (The artifact results from sharp peaks at both ends of each projection (*5*, *8*).) The resolution, however, may be somewhat lowered due to the interpolation made in the *k*-space. Of course, no phase twist can be observed.

The same experiments have been extended to the adamantane and polycarbonate samples, both consisting of two blocks as depicted in Fig. 4. These samples are much closer to rigid solids than the natural rubber sample, enabling much more critical experimental tests of the symmetric echo acquisition.

Figure 4 shows the results of the 2D imaging experiments performed on the adamantane sample. The images, 4a and 4b, were obtained by FBP while the image, 4c, was computed by 2D FT. Except for sensitivity, the echo-FT absolute-value image, 4b, looks essentially the same as the FID-FT real image, 4a, indicating that a highly symmetric echo was acquired again in this sample. This can be expected naturally from the high degree of line narrowing achieved in this particular sample (T_2 lengthened from 50 μs to 15 ms). However, a similarly symmetric echo acquisition was realized in the polycarbonate sample as well, where only a moderate line narrowing was obtained under the same experimental conditions (T_2 lengthened from 30 μs to 1.5 ms). The high symmetry of the echo acquired under the moderate line narrowing is due to the sophisticated way of acquisition and may be difficult to obtain with the simple echo acquisition (*2*). This advantage of the sophisticated acquisition is confirmed by the close resemblance of the 1D images of the polycarbonate sample shown in Fig. 5. The FID-FT real projection is displayed as 5a and the echo-FT absolute-value projection as 5b.

The sophisticated echo acquisition was considered analogously with that performed in liquid-state MRI using the CPMG spin-echo sequence (*17*). Although the analogy appears to be simple, certain experimental imperfections in the TREV-16TS sequence may severely damage the sophisticated acquisition under the line narrowing. During all the experiments, therefore, we tried to find experimental parameters for the TREV-16TS imaging sequence that were critical for the symmetric echo acquisition. It was found that the nutation of the magnetization during the sandwiched RF irradiation (see Fig. 1a) is sensitive to the successful echo acquisition. In particular, the nutations associated with the phase-reversed (x and $-x$) RF irradiations must be canceled; namely, the net nutation angle during the 4τ irradiations must be zero. This was very critical: Even a 1% imbalance for the cancelation immediately led to an apparently distorted absolute-value projection image. It was adjusted by observing the in-phase signal so that the difference between the odd- and even-numbered echo amplitudes is minimized. The other parameters do not appear to be so critical. The flip-angle adjustment of 90° pulses, for example, was much less critical; even an upto about 10% misadjustment did not lead to a significant image distortion for the natural rubber sample.

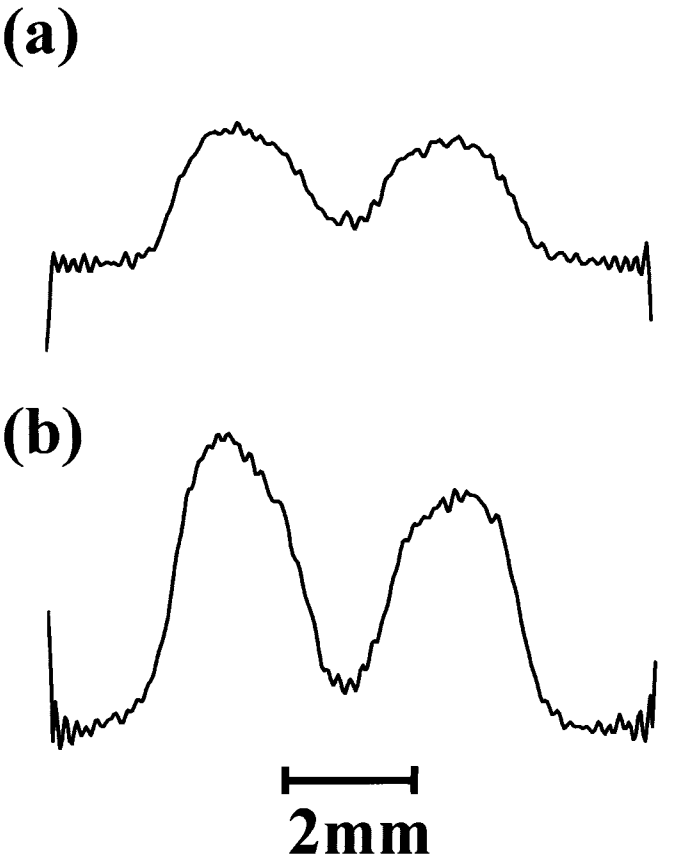

FIG. 5. One-dimensional images (projections) of the polycarbonate sample consisting of two blocks as shown by the inset in Fig. 4. (a) FID-FT real and (b) echo-FT absolute-value projections. The close resemblance of these projections indicates that a highly symmetric echo was acquired for the polycarbonate sample, where only a moderate line narrowing was obtained (T_2 lengthened from 30 μs to 1.5 ms). Also, the sensitivity improvement in the echo-FT imaging is evident. The sharp peaks at both ends of the projections are artifacts.

CONCLUSION

We have demonstrated that by modifying the gradient sequence in the TREV-16TS solid-state imaging, it becomes possible to acquire a symmetric echo signal that can be used for the high-resolution absolute-value image display after the echo FT. This improves the performance of the TREV-16TS solid-state imaging: the $\sqrt{2}$ gain in sensitivity, the nonnecessity for the phase correction, and the doubled digital resolution. These advantages have been confirmed by the 1D and 2D imaging experiments performed on the three test samples. The experiments have also disclosed the TREV16-TS adjustment parameter that is critical for the successful echo acquisition. We hope that the improved performance of magic-echo solid-state imaging will further activate the application of solid-state imaging to material characterization.

ACKNOWLEDGMENTS

We thank Dr. Tamon Inouye (Professor Emeritus, University of Tsukuba and President, Institute for Applied Mathematics, Inc.) for encouragement. Thanks are also due to Dr. Takeyuki Hashimoto of Yokohama Souei College for helpful suggestions on the *k*-space interpolation. Dr. Masayuki Nonaka of Hitachi Medical Corporation kindly assisted on some of the experiments.

REFERENCES

1. A. Bax, A. L. Mehlkopf, and J. Smidt, *J. Magn. Reson.* **35,** 373–377 (1979).
2. G. C. Chingas, J. B. Miller, and A. N. Garroway, *J. Magn. Reson.* **66,** 530–535 (1986).
3. S. Matsui, *Chem. Phys. Lett.* **179,** 187–190 (1991).
4. S. Matsui, *J. Magn. Reson.* **95,** 149–153 (1991).
5. S. Matsui, *J. Magn. Reson.* **98,** 618–621 (1992).
6. S. Matsui, Y. Ogasawara, and T. Inouye, *J. Magn. Reson. A* **105,** 215–218 (1993).
7. S. Matsui, A. Uraoka, and T. Inouye, *J. Magn. Reson. A* **112,** 130–133 (1995).
8. S. Matsui, A. Uraoka, and T. Inouye, *J. Magn. Reson. A* **120,** 11–17 (1996).
9. S. Matsui, M. Nonaka, T. Nakai, and T. Inouye, *Solid State NMR* **10,** 39–44 (1997).
10. S. Matsui, M. Nonaka, T. Nakai, and T. Inouye, *J. Magn. Reson.* **138,** 220–224 (1999).
11. M. Nonaka, S. Matsui, and T. Inouye, *J. Magn. Reson.* **145,** 315–318 (2000).
12. F. Weigand, B. Blümich, and H. W. Spiess, *Solid State NMR* **3,** 59–66 (1994).
13. M. L. Buszko and G. E. Maciel, *J. Magn. Reson. A* **107,** 151–157 (1994).
14. M. A. Hepp and J. B. Miller, *J. Magn. Reson. A* **111,** 62–69 (1994).
15. W.-K. Rhim, A. Pines, and J. S. Waugh, *Phys. Rev. B* **3,** 684–695 (1971).
16. K. Takegoshi and C. A. McDowell, *Chem. Phys. Lett.* **116,** 100–104 (1985).
17. D. J. O. McIntyre, F. Hennel, and P. G. Morris, *J. Magn. Reson.* **130,** 58–62 (1998).